

Generation of orbital angular momentum hologram using a modified U-net

Zhi-Gang Zheng(郑志刚), Fei-Fei Han(韩菲菲), Le Wang(王乐), and Sheng-Mei Zhao(赵生妹)

Citation: Chin. Phys. B, 2024, 33 (**3**): 034207. DOI: 10.1088/1674-1056/ad12aa
Journal homepage: http://cpb.iphy.ac.cn; http://iopscience.iop.org/cpb

What follows is a list of articles you may be interested in

Bessel—Gaussian beam-based orbital angular momentum holography

Jiaying Ji(季佳滢), Zhigang Zheng(郑志刚), Jialong Zhu(朱家龙), Le Wang(王乐), Xinguang Wang(王新光), and Shengmei Zhao(赵生妹)
Chin. Phys. B, 2024, 33 (**1**): 014204. DOI: 10.1088/1674-1056/acfdff

Tailoring OAM spectrum of high-order harmonic generation driven by two mixed Laguerre-Gaussian beams with nonzero radial nodes

Beiyu Wang(汪倍羽), Jiaxin Han(韩嘉鑫), and Cheng Jin(金成)
Chin. Phys. B, 2023, 32 (**12**): 124208. DOI: 10.1088/1674-1056/ad0144

Diffraction deep neural network based orbital angular momentum mode recognition scheme in oceanic turbulence

Hai-Chao Zhan(詹海潮), Bing Chen(陈兵), Yi-Xiang Peng(彭怡翔), Le Wang(王乐), Wen-Nai Wang(王文鼐), and Sheng-Mei Zhao(赵生妹)
Chin. Phys. B, 2023, 32 (**4**): 044208. DOI: 10.1088/1674-1056/ac935e

Asymmetrical spiral spectra and orbital angular momentum density of non-uniformly polarized vortex beams in uniaxial crystals

Ling-Yun Shu(舒凌云), Ke Cheng(程科), Sai Liao(廖赛), Meng-Ting Liang(梁梦婷), and Ceng-Hao Yang(杨嶒浩)
Chin. Phys. B, 2023, 32 (**2**): 024211. DOI: 10.1088/1674-1056/ac7860

Up-conversion detection of mid-infrared light carrying orbital angular momentum

Zheng Ge(葛正), Chen Yang(杨琛), Yin-Hai Li(李银海), Yan Li(李岩), Shi-Kai Liu(刘世凯), Su-Jian Niu(牛素俭), Zhi-Yuan Zhou(周志远), and Bao-Sen Shi(史保森)
Chin. Phys. B, 2022, 31 (**10**): 104210. DOI: 10.1088/1674-1056/ac6eda

---

Generation of orbital angular momentum hologram using a modified U-net

Zhi-Gang Zheng(郑志刚)[1], Fei-Fei Han(韩菲菲)[1], Le Wang(王乐)[1], and Sheng-Mei Zhao(赵生妹)[1,2,3,†]

[1] *Institute of Signal Processing and Transmission, Nanjing University of Posts and Telecommunications, Nanjing* 210003, *China*
[2] *Key Laboratory of Broadband Wireless Communication and Sensor Network Technology (Ministry of Education), Nanjing University of Posts and Telecommunications, Nanjing* 210003, *China*
[3] *National Laboratory of Solid State Microstructures, Nanjing University, Nanjing* 210093, *China*

(Received 29 October 2023; revised manuscript received 4 December 2023; accepted manuscript online 6 December 2023)

Orbital angular momentum (OAM) holography has become a promising technique in information encryption, data storage and opto-electronic computing, owing to the infinite topological charge of one single OAM mode and the orthogonality of different OAM modes. In this paper, we propose a novel OAM hologram generation method based on a densely connected U-net (DCU), where the densely connected convolution blocks (DCB) replace the convolution blocks of the U-net. Importantly, the reconstruction process of the OAM hologram is integrated into DCU as its output layer, so as to eliminate the requirement to prepare training data for the OAM hologram, which is required by conventional neural networks through an iterative algorithm. The experimental and simulation results show that the OAM hologram can rapidly be generated with the well-trained DCU, and the reconstructed image's quality from the generated OAM hologram is significantly improved in comparison with those from the Gerchberg–Saxton generation method, the Gerchberg–Saxton based generation method and the U-net method. In addition, a 10-bit OAM multiplexing hologram scheme is numerically demonstrated to have a high capacity with OAM hologram.

Keywords: orbital angular momentum (OAM), holography, OAM holography, deep learning

PACS: 42.40.–i, 42.50.Tx, 42.79.Sz, 84.35.+i **DOI:** 10.1088/1674-1056/ad12aa

1. Introduction

Orbital angular momentum (OAM) is demonstrated by a helical wavefront beam with $\exp(\mathrm{i}l\varphi)$,[1] where l is a topological charge and φ is an azimuthal angle and has been applied as an information carrier in optical communication,[2–6] quantum information,[7–9] *etc*. Recently, holography based on OAM has received growing interest for its large capacity in information encryption, data storage and opto-electronic computing.[10–12]

For holography, the generation of its computer-generated hologram (CGH) is an important part, and many methods have been proposed and demonstrated.[13–16] For example, the Gerchberg–Saxton (GS) algorithm, an iterative phase retrieval algorithm widely employed in beam shaping and optical information processing, was employed for calculating the hologram,[13,14] and the OAM hologram.[10–12] However, the random initial phase at the beginning of the algorithm leads to the speckle noise in the reconstructed image. Thereafter, a double-constraint GS method was proposed in which the required phase information and amplitude information were limited in the image plane in each iteration, as opposed to utilizing random phase.[15] Consequently, this method suppressed the speckle noise brought by the random phase. Then, a method called random phase-free CGH was proposed to enhance image quality and reduce the speckle noise by multiplying the object light with the virtual convergence light.[16] A random repeated and displaced phase was proposed by using a structured random phase. The full image was reconstructed with reduced speckle noise from a partially illuminated Fresnel hologram.[17] However, these methods require either parameter adjustments for different input images or intricate computations.

To reduce the speckle noise of the holographic reconstructed images, deep learning (DL),[18,19] the artificial intelligence technique, has been recently adopted in hologram generation. For instance, in order to reduce the speckle noise for coherent imaging without clean data, Yin *et al.* proposed a hologram generation method to combine the traditional GS technique with the convolutional neural network (CNN).[20] Based on the combination of the U-net and a diffraction propagation model, Sun *et al.* presented a phase hologram generation method based on CNN to suppress the speckle noise of the reconstructed image.[21] By combining the random phase-free method with the scaled diffraction computation, Ishii *et al.* proposed a DL-based CGH optimization method for holographic projection and demonstrated that the reconstruction result outperformed those with GS algorithm.[22] However, these studies either optimize a single image, that is, the network cannot predict images that have not been trained before, or require extensive time to prepare the training data. Importantly, OAM holography has some characteristics, such as us-

†Corresponding author. E-mail: zhaosm@njupt.edu.cn
© 2024 Chinese Physical Society and IOP Publishing Ltd

ing point images to preserve the OAM property, and the work to generate an OAM hologram directly by using a deep neural network has not been discussed yet.

In this paper, we propose an OAM hologram generation method based on a densely connected U-net (DCU) with a new training strategy, where DCU is a modified U-net discussed in detail in Refs. [23–25] and U-net is a well-established encode and decode network architecture, which has been widely used for regression tasks. In DCU, the densely connected convolution blocks (DCB) are specially designed to replace the convolution blocks in the traditional U-net. The reconstruction process of the OAM hologram is integrated into the output layer of DCU, so there is no requirement to prepare the training data for the OAM hologram by using the other method, say, the GS algorithm. A special loss function is designed to optimize the background part and the signal part of input images, respectively. The numerical simulation and the experiment are performed to demonstrate the feasibility of the proposed method and the performance of the reconstructed image. In addition, the application of the generated OAM multiplexing hologram in optical encryption is discussed.

The organization of the paper is the following. The theory is introduced in Section 2. In Section 3, the performance of the proposed method is verified, and the conclusion is summarized in Section 4.

2. Theory

OAM is applied as a novel information carrier for holography due to its good properties, such as the infinite values of its topological charge, and the orthogonality between different OAM modes. To preserve the characteristics of OAM in holography, the target image should be multiplied with a two-dimensional (2D) sampling array in the image plane, say, the point image, whose sampling interval is dependent on the spatial frequency of the used OAM mode.[10]

As the input images for the proposed method are point images, it is essential to acquire high signal-to-noise (SNR) information at the sampling points as well as low SNR information in the background part by the network. Hence, the structure of the DL for the OAM hologram generation method should be designed. Figure 1 shows the schematic diagram of the proposed method to generate the OAM hologram, where the target image is first multiplied by a sampling array, then the point image is used as the "input image" of DCU, and the output of the network is the predicted OAM-preserved hologram, named "output hologram". To avoid the preparation of the training data for hologram as conventional DL-based hologram generation methods by the iterative algorithm, the reconstruction process of the OAM hologram is included as the output layer of the overall network which reduces the difficulty of obtaining training data. The predicted OAM hologram is calculated as the "reconstruction", and the "reconstruction", which together with the "input image" serve as the training data for the proposed network. Especially, a loss function is designed for the proposed network to obtain a high-quality reconstruction from the OAM hologram.

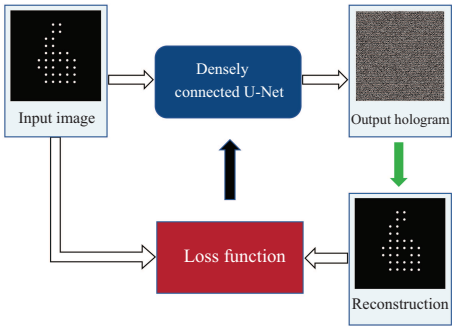


Fig. 1. The schematic diagram of the proposed method. The white arrow represents the data transmission, the black arrow represents the data fed back into the neural network, and the green arrow represents the reconstruction process of the OAM hologram.

Then, the densely connected U-net and the loss function are described in detail as follows.

2.1. Densely connected U-net

The structure of the DCU is shown in Fig. 2, where the convolution blocks in U-net are replaced by the DCBs[26] to overcome the vanishing gradient problem during the training process of DCU. The structure of DCU consists of a shrinking path on the left, a spreading path on the right, and a bottleneck layer in the middle. The numbers on the left side of the DCBs are the dimensions of the feature map. The white arrow in the bottleneck layer represents data transmission, while the red arrow in the shrinking path represents down-sampling, and the blue arrow in the spreading path represents transposed convolution. The purpose of the shrinking path is to encode the feature information of the input space into a higher-dimensional feature space. The structure of the spreading path is identical to that of the shrinking path, and its purpose is to extend and decode the extracted feature map to the output space using the multi-layer transposed convolution layer. The bottleneck layer is used to transmit the recorded information from the DCBs in the shrinking path to its matched decoder DCBs in the spreading path. Therefore, the extracted feature information is considerably enhanced by the bottleneck layer. A DCB is further illustrated by the blue box in Fig. 2. There are 3 layers inside, one after the other are in a feed-forward fashion. The feature maps of all proceeding layers are used as inputs, and their own feature maps are used as inputs into all subsequent layers. Here, each layer consists of the convolution layer, batch normalization (BN), and activation function.

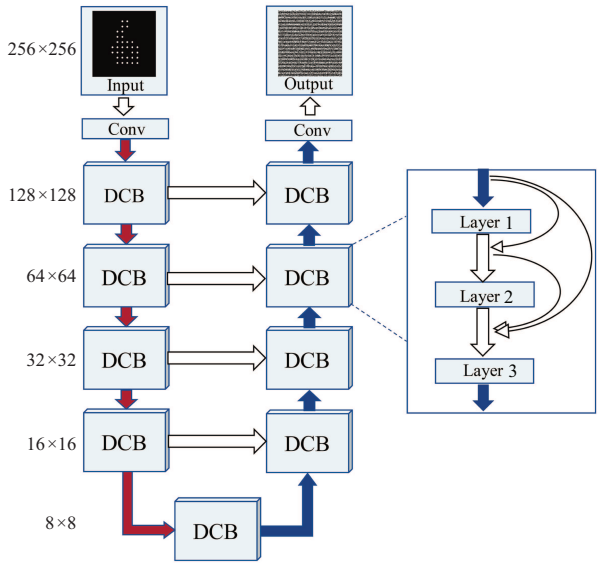


Fig. 2. The schematic diagram of the densely connected U-net. The white arrow represents data transmission, while the red arrow represents down-sampling and the blue arrow represents transposed convolution. The details of one DCB are shown in the blue box.

The operation from the $(l-1)$-th layer to the l-th layer can be expressed as

$$y_j^l = \sigma\left(\sum_{i\in T_j^{l-1}} W_{ij}^l y_i^{l-1} + b_j^l\right), \tag{1}$$

where y_i^{l-1} represent the output of the i-th neuron in the $(l-1)$-th layer and y_j^l represent the output of the j-th neuron in the l-th layer. T_j^{l-1} is the number of feature maps in the $(l-1)$-th convolution layer and W_{ij}^l is the weights that can be learned and updated in the convolution kernel in the l-th layer. b_j^l represents the bias in the j-th feature map of the l-th layer, and $\sigma(\cdot)$ represents the adopted activation function. For each layer in one DCB, the input of the current layer is represented by the superposition of the output of all previous layers, which can be expressed as

$$y^l = H_l(y^0, y^1, \ldots, y^{l-1}), \tag{2}$$

where H_l is a nonlinear transformation function related with the operations in Eq. (1) and $y^0, y^1, \ldots, y^{l-1}$ mean the output of all the layers before the l-th layer. The densely connected mechanism not only plays a central role in strengthening feature information reuse but also performs an excellent job of integrating the high SNR information and low SNR information of input images during the network training. Therefore, it can obtain accurate information on input images.

In this paper, each convolution layer uses a kernel size of 3×3, a step size of 2, and a padding of 0. The output image size of the down-sampling layer is exactly half of the input size. In order to introduce nonlinearity, rectified linear unit (ReLU) which is an activation function commonly used in neural networks is employed, while BN is adopted to speed up and stabilize the network's training.

2.2. Loss function

To obtain a better convergence effect of the network, the target image is divided into two parts, the signal part and the background part by applying a binary mask. The binary mask is defined as

$$\mathrm{Mask}(x,y) = \begin{cases} 1, & A(x,y) > \text{threshold}, \\ 0, & A(x,y) \le \text{threshold}, \end{cases} \tag{3}$$

where $A(x,y)$ represents the amplitude intensity value of the target image at the position (x,y). Here, the criterion for the threshold is that the signal part is located in the middle of the target image, and its size is slightly larger than that of the signal part.

The squared L2 norm is served as the loss function to calculate the loss of the signal part and background part, and the whole loss function includes the two parts' loss functions, which is expressed as

$$\mathrm{Loss}_{\mathrm{sum}} = \|\varphi_{\mathrm{r}} - \varphi_{\mathrm{t}}\|_2^2 + \beta\,\|\varphi_{\mathrm{rb}} - \varphi_{\mathrm{tb}}\|_2^2, \tag{4}$$

where $\|\cdot\|_2^2$ is the squared L2 norm, φ_{tb} and φ_{t} denote grayscale values of the background part and the signal part of the input image, respectively; φ_{rb} and φ_{r} denote grayscale values of the background part and the signal part of the reconstructed image from the output OAM hologram, respectively. The parameter β (0–1) is applied to adjust the optimization ratio of the signal part and the background part. For a smaller value β, it is indicated that the training process prefers to optimize the signal part, while for a larger value, it is indicated that the training process seeks to optimize the background part. The difference between the reconstructed images from the predicted OAM hologram and the ground truth can be reduced with the use of the back-propagation of the loss function. Then, ADAM optimizer which is a method for stochastic optimization is applied as the updating rule to minimize the total loss function $\mathrm{Loss}_{\mathrm{sum}}$. The weight and bias of the network can be automatically updated in each epoch. Based on this updating rule, the optimization process can reach the global minimum when the total loss function is converged, and the well-trained network can predict the optimal OAM hologram for an input image.

3. Results and discussion

In this paper, to statistically analyze the result, the structural similarity index metric (SSIM), the peak signal-to-noise ratio (PSNR)[27] and the cosine similarity (CS)[28] are adopted. SSIM is an index to measure the similarity of two images, its mathematical expression is

$$\mathrm{SSIM}(X,Y) = \frac{(2\mu_X\mu_Y + c_1)(2\sigma_{XY} + c_2)}{(\mu_X^2 + \mu_Y^2 + c_1)(\sigma_X^2 + \sigma_Y^2 + c_2)}, \tag{5}$$

where μ_X and μ_Y represent the average value of the input image and the reconstructed image respectively, σ_X and σ_Y are the variances, and σ_{XY} are the covariance between the two images. $c_1 = (\alpha \times N)^2$ and $c_2 = (\beta \times N)^2$ denote the regularization parameter, where $\alpha = 0.01$, $\beta = 0.03$, and $N = 255$ (the range of pixel values).

The PSNR is also a metric to qualify an image and its mathematical expression is

$$\mathrm{PSNR} = 10 \times \log_{10}\left(\frac{\mathrm{MAX}_{\mathrm{val}}^2}{\mathrm{MSE}}\right), \tag{6}$$

where $\mathrm{MAX}_{\mathrm{val}}$ denotes the maximum gray value in the image and MSE is the mean square error between input image and reconstructed image, which is defined as

$$\mathrm{MSE} = \frac{1}{M \times N}\sum_{x,y}[\varphi_X(x,y) - \varphi_Y(x,y)]^2, \tag{7}$$

where $\varphi_X(x,y)$ and $\varphi_Y(x,y)$ are the grayscale values of the input image and the reconstructed image at the position (x,y), respectively. M and N denote the number of pixels in the horizontal and vertical directions of the input image, respectively.

Cosine similarity (CS) is a measure of similarity between two vectors of an inner product space that measures the cosine of the angle between them and its expression is

$$\mathrm{CS} = \frac{\sum_{i=1}^{n}(m_i \times h_i)}{\sum_{i=1}^{n}(m_i)^2 \times \sum_{i=1}^{n}(h_i)^2}, \tag{8}$$

where $\boldsymbol{m}$ and $\boldsymbol{h}$ denote two distinct vectors and n is the length of the vector. Considering the pixel information in the reconstructed image may be shifted in the positions, we employ visual geometry group (VGG) to extract the image features at first, then we compute the CS values on the image feature vectors.

3.1. Numerical simulation

In this section, we first verify the performance of the proposed method through numerical simulations. The images input to the designed network for training and testing are from the modified handwritten digital database of the Modified National Institute of Standards and Technology (MNIST), including the handwritten digits[29] and the Fashion-MNIST.[30] The training dataset and testing dataset consist of 6×10^4 and 1×10^4 greyscale images, respectively. The images are with a resolution of 256×256 pixels, and the size of each pixel is 12.5 μm × 12.5 μm considering the optical experimental setup. The shrinking path and the spreading path both consist of five DCBs and each block contains 3 layers.

The threshold of the mask is set to 0.5, and the value of β is 0.1. The ADAM optimizer's learning rate is set to 0.001. Considering the limitations of time cost and training memory, each batch includes 32 input images. The neural network is implemented based on Python 3.10.0, and PyTorch is employed to build the network structure on NVIDIA TITAN RTX GPU with CUDA version 11.4. It takes approximately 10 h to complete 50 epochs of training.

First, we demonstrate the feasibility of the proposed method. In previous works, U-net is already applied to generate holograms.[21] In order to analyze different OAM hologram generation methods, we compare the qualities of the reconstructed OAM holographic images by the proposed method, the GS[13] method, the weighted Gerchberg–Saxton (WGS)[31] method, the adaptive weighted Gerchberg–Saxton (AWGS)[32] method, and the U-net method in Table 1. The neural network in the U-net method is roughly equivalent to those applied in the proposed method in terms of the number of network layers. The number of iterations for the GS method and its improved versions are the same. The results show that the values of SSIM and PSNR of the reconstructed holographic images by the proposed method are up to 0.9945 and 47.7971 for the MNIST dataset, while they are 0.9923 and 44.4406 for the Fashion-MNIST dataset, which are higher than those with the GS based methods and the U-net method. It is indicated that the proposed method can obtain a higher-quality OAM hologram in comparison with the GS method, GS based method and U-net method. Additionally, for the Fashion-MNIST, it only takes 53.2 milliseconds to generate a 256×256 pixels OAM hologram by utilizing the proposed method, while it takes 4.96 seconds for the commonly used WGS method, it indicates that the proposed method can quickly generate an OAM hologram.

Table 1. SSIM and PSNR values of the proposed method, GS method, WGS method, AWGS method and U-net method.

	SSIM		PSNR	
	MNIST	Fashion-MNIST	MNIST	Fashion-MNIST
Proposed method	0.9945	0.9923	47.7971	44.4406
GS method	0.9905	0.9797	46.0061	41.1590
WGS method	0.9906	0.9784	46.0228	42.8080
AWGS method	0.9874	0.9770	43.4051	40.3551
U-net method	0.9717	0.9807	41.3183	41.0470

Figure 3 further shows the training loss versus the epochs for the proposed method and the U-net method. It is shown that for the proposed method, the training and validation loss are both fall down quickly in the first five epochs, and then they gradually converge to lower loss values after 30 epochs, say 0.01. It hint that the proposed method has a good training effect with the designed network architectures. For the U-net method, the validation loss has a fluctuation, and the initial and final training loss values are bigger than those by the proposed method, which also means that the network in the

proposed method has a better fitting performance and faster convergence.

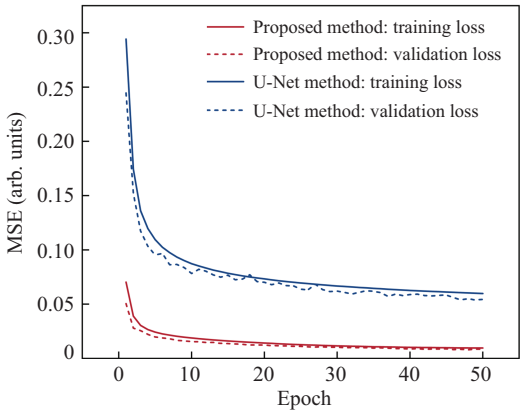


Fig. 3. Training and validation loss curves of the proposed method and the U-net method.

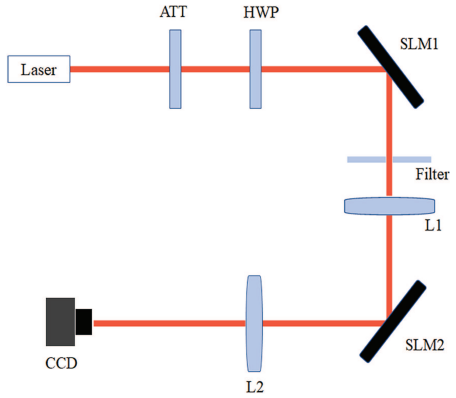


Fig. 4. The experimental setup of the proposed method. ATT: attenuator; HWP: half-wave plate; SLM: spatial light modulator; L1: lens (the focal length 150 mm); L2: lens (the focal length 50 mm); CCD: charge coupled device.

3.2. Optical experiment

To further evaluate the performance of the proposed method, we discuss the experimental results of the OAM hologram. Figure 4 shows the experimental schematic diagram of the proposed method. In the experiment, the He–Ne laser (Thorlabs, HRS015) emits a linear fundamental mode Gaussian beam with a wavelength of 633 nm. The Gaussian beam passes through an attenuator (ATT) to adjust the power of the beam. An half-wave plate (HWP) is then employed to adjust the Gaussian beam to an appropriate polarization to match the spatial lighter modulator (SLM1,PLUTO-VIS-006-A, pixel pitch: 8 μm, pixel number: 1920×1080). The filter is employed to ensure that there is only the first-order of the vortex beam is retained. Lens L1 (the focal length 150 mm) is employed to focus the vortex beam on SLM2 (HED6010-NIR-011-C, pixel pitch: 8 μm, pixel number: 1920×1080), which carries predicted OAM holograms obtained by the proposed method. Lens L2 (the focal length 50 mm) is a Fourier lens to focus the distribution of beam intensity on a CCD (Thorlabs, BC106N-VIS/M), which records the intensity distribution of the reconstructed OAM hologram. Firstly, we load a helical phase structure on SLM1, and none on SLM2 to get different OAM incident beams. At this time, the image recorded in the CCD is a doughnut structure. Then, we load the predicted OAM holograms, including the OAM-selective hologram and the OAM-multiplexing hologram on SLM2. At this time, the image recorded in the CCD is the holographic reconstructed image.

Figure 5 shows the reconstructed holographic images with the proposed method, the GS method, the WGS method, the AWGS method, and the U-net method, respectively. The ground truth images are from MNIST dataset, including "1", "7", and "8" three handwritten digits images, and from Fashion-MNIST dataset, including "overcoat" and "trouser" images. Here, the OAM-selective holograms are produced by superimposing a helical phase plate of $l = -1$ on the OAM-preserved hologram, and the reconstructed image emerges only when $l = 1$ OAM incident beam is employed. From the results, one can see that the OAM holographic reconstruction results by the proposed method match well with the ground truth. From the red boxes in Fig. 5, it is evident that the image information is reconstructed completely by the proposed method, in comparison with those results obtained by the GS method, the GS based methods and the U-net method.

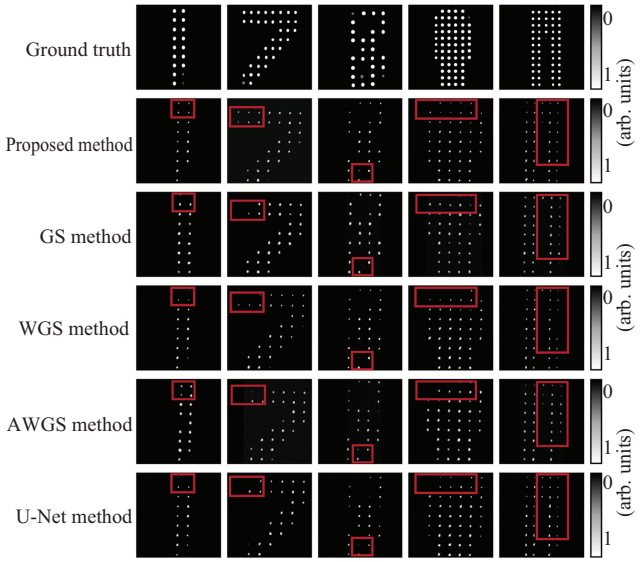


Fig. 5. The experimental results of OAM-multiplexing holographic reconstructed images.

To quantitatively compare the five methods' results in the experiment, the CS values are adopted for the consideration of the pixel information shifting in the reconstructed images. Table 2 shows the comparison of CS values of the proposed method, GS method, the GS based methods and the U-net method, respectively, from the experimental results. The results show that the proposed method has highest CS values for three handwritten digits images from MNIST dataset and

"trouser" images from Fashion-MNIST dataset except for the "overcoat" images, it indicates that the proposed method is able to accomplish high quality reconstruction.

Table 2. The comparison of CS values of the proposed method, GS method, WGS method, AWGS method and U-net method from the experimental results.

	"1"	"7"	"8"	Overcoat	Trouser
Proposed method	0.861	0.862	0.823	0.788	0.844
GS method	0.801	0.713	0.745	0.729	0.789
WGS method	0.849	0.630	0.798	0.808	0.778
AWGS method	0.747	0.535	0.720	0.668	0.772
U-net method	0.856	0.575	0.777	0.841	0.837

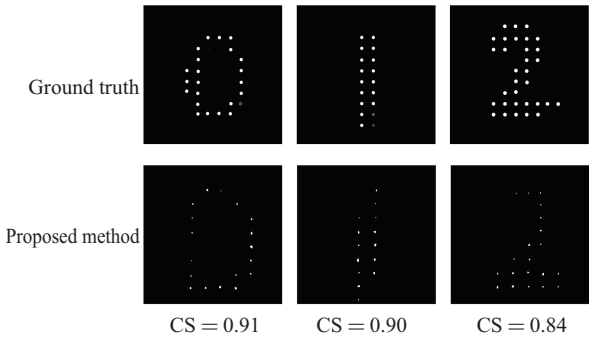


Fig. 6. The experimental results of OAM-selective holographic reconstructed images.

Additionally, we demonstrate the experimental results of the OAM-multiplexing hologram generated by the proposed method in Fig. 6. Three independent OAM channels are prepared for the three handwritten digits "0", "1", and "2", respectively. The OAM-multiplexing hologram is generated by the superposition of multiple OAM-selective holograms with $l = -1, 1, 2$. The handwritten digits "0", "1", and "2" are reconstructed by applying the OAM beams with $l = 1, -1, -2$ to illuminate the OAM-multiplexing hologram, respectively. The CS values for the reconstructed images are calculated. The experimental results demonstrate that the proposed method can effectively generate an OAM-multiplexing hologram, and the reconstructed results of the OAM-multiplexing hologram are consistent with the ground truth. The CS values are 0.91, 0.90, and 0.84 for digits "0", "1", and "2" respectively.

3.3. Application in encryption

In this subsection, we discuss the application of the OAM-multiplexing hologram generated by the proposed method. Here, we present a 10-bit encryption scheme based on the proposed OAM-multiplexing hologram by numerical simulation. As shown in Fig. 7(a), OAM topological charge values from -25 to 25 are employed to encode 10 digital characters (0–9) with a capacity of 10 bit. This enables the implementation of an OAM encryption scheme. Digits "0", "1", "2", …, "9" are first sampled with an OAM-dependent sampling array in the image plane so that the corresponding OAM-preserved hologram for ten digits can be obtained. Then the helical phase plates with the designed topological charge values, such as $\ell = -25$, $\ell = -20$, …, $\ell = 25$, are sequentially added to each OAM-preserved hologram to achieve the OAM-selective hologram. The OAM-multiplexing hologram is obtained by superposing all the OAM-selective holograms. The 10-bit OAM-multiplexing hologram is used as the ciphertext of this scheme and different digital images are reconstructed when different incident OAM beam is illuminated.

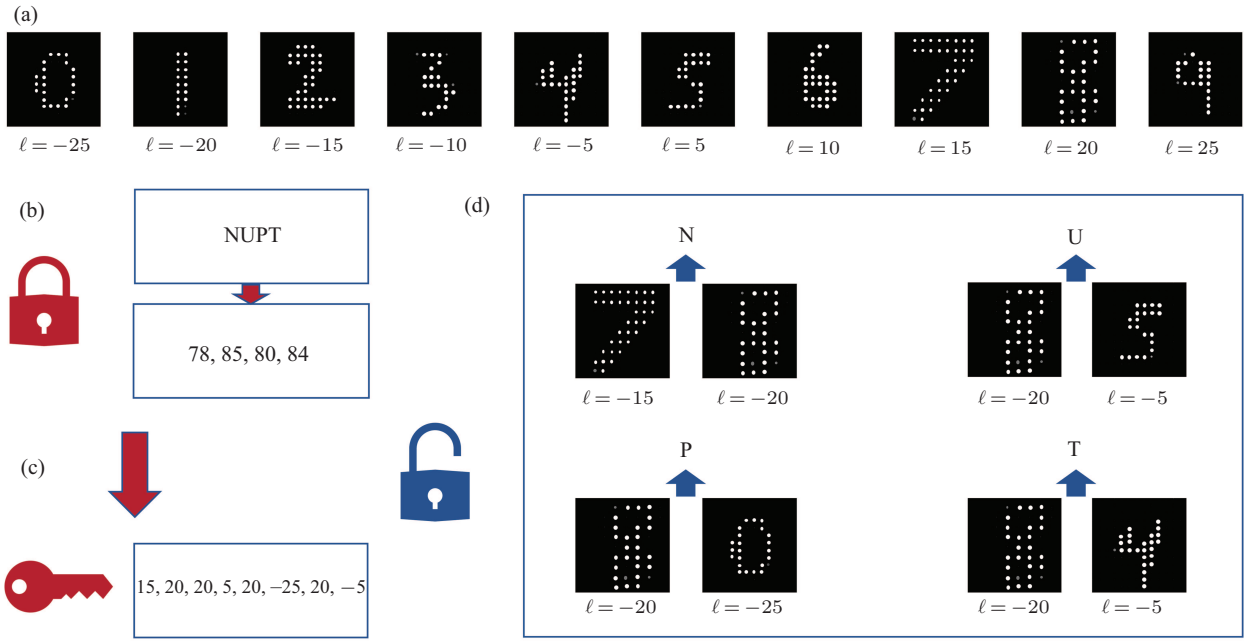


Fig. 7. The schematic diagram of a 10-bit OAM holography encryption scheme.

For the English letters "NUPT", the message to be encrypted in Fig. 7(b), each letter of the "NUPT" is first converted to its corresponding ASCII as "78, 85, 80, 84", so that the corresponding OAM topological charge values are $l = (15\ 20, 20\ 5, 20\ -25, 20\ -5)$ serving as the key to the encryption scheme, as shown in Fig. 7(c). In the decryption, the corresponding incident OAM beam with inverse topological charge value is first generated according to the key and then sequentially illuminating the OAM-multiplexing hologram. Finally, each of the four digital combinations is obtained through the reconstructed images, and the English letters "NUPT" are recovered by the ASCII, as shown in Fig. 7(d). When the key is lost, the encrypted information cannot be recovered. The results demonstrate that the multiplexing of OAM-selective holograms with a helical mode index from -25 to 25 has led to 10-bit OAM-encoded holograms for high-security encryption which demonstrates a high-capacity holographic encryption system.

4. Conclusion

In this paper, we have proposed a modified U-net-based OAM hologram generation method, where the densely connected U-net has been trained to learn the correspondence between the input images and their OAM holograms. The reconstruction process of the OAM hologram is integrated into DCU architecture as its output layer so as to eliminate the need to prepare training data, reducing the difficulty of acquiring training data as in conventional neural networks. The numerical simulation and experimental results have shown that the qualities of the generated OAM holograms and their reconstructed images have been improved by the proposed method, and the time required to generate an OAM hologram is greatly reduced with the well-trained densely connected U-net. In addition, a 10-bit OAM holography encryption scheme has been implemented by employing the proposed OAM hologram generation method, and the results have shown that the designed OAM holographic encryption scheme is available and secure. Our method provides a novel way for designing OAM holograms and may be used in holographic encryption and data storage.

Acknowledgements

This work was supported by the National Natural Science Foundation of China (Grant Nos. 62375140 and 61871234) and the Open Research Fund of National Laboratory of Solid State Microstructures (Grant No. M36055).

References

[1] Allen L, Beijersbergen M W, Spreeuw R J C and Woerdman J P 1992 *Phys. Rev. A* **45** 8185
[2] Willner A E, Huang H , Yan Y, Ren Y, Ahmed N, Xie G, Bao C, Li L, Cao Y, Zhao Z, Wang J, Lavery M P J, Tur M, Ramachandran S, Molisch A F, Ashrafi N and Ashrafi S 2015 *Adv. Opt. Photon.* **7** 66
[3] Zou L, Wang L, Zhao S M and Chen W W 2016 *Chin. Phys. B* **25** 114215
[4] Zhan H C, Chen B, Peng Y X, Wang L, Wang W N and Zhao S M 2023 *Chin. Phys. B* **32** 044208
[5] Ji J Y, Zheng Z G, Zhu J L, Wang L, Wang X G and Zhao S M 2023 *Chin. Phys. B*
[6] Zhu J L, Wang L, Ji J Y and Zhao S M 2022 *Appl. Phys. Lett.* **120** 251104
[7] Mair A, Vaziri A, Weihs G and Zeilinger A 2001 *Nature* **412** 313
[8] Fickler R, Lapkiewicz R, Plick N W, Krenn M, Schaeff C, Ramelow S and Zeilinger A 2012 *Science* **338** 6107
[9] Fickler R, Campbell G, Buchler B, Ping K L and Zeilinger A 2016 *PANS* **113** 13642
[10] Fang X Y, Ren H R and Gu M 2020 *Nat. Photon.* **14** 102
[11] Ren H, Briere G, Fang X, Ni P, Sawant R, Heron S, Chenot S, Vezian S, Damilano B, Brandli V and Genevet P 2019 *Nat. Commun.* **10** 2986
[12] Zhou H Q, Wang Y T, Li X, Xu Z T, Li X and Huang L L 2021 *Appl. Phys. Lett.* **119** 044104
[13] Gerchberg R W 1972 *Optik* **35** 237
[14] Wu Y, Wang J, Chen C, Liu C J, Jin F M and Chen N 2021 *Opt. Express* **29** 1412
[15] Chang C L, Xia J, Yang L, Lei W, Yang Z M and Chen J H 2015 *Appl. Opt.* **54** 6994
[16] Shimobaba T and Ito T 2015 *Opt. Express* **23** 9549
[17] Cruz M L 2019 *Appl. Opt.* **58** 1917
[18] LeCun Y, Bengio Y and Hinton G 2015 *Nature* **521** 436
[19] Lucas A, Iliadis M, Molina R and Katsaggelos A K 2018 *IEEE Signal Processing Mag.* **35** 20
[20] Yin D, Gu Z, Zhang Y, Gu F, Nie S, Feng S and Yuan C 2020 *Opt. Lasers Eng.* **133** 106151
[21] Sun X H, Mu X Y, Xu C, Pang H, Deng Q L, Zhang K, Jiang H B, Du J L, Yin S Y and Du C L 2022 *Opt. Express* **30** 2646
[22] Ishii Y, Shimobaba T, Blinder D, Birnbaum T, Schelkens P, Kakue T and Ito T 2022 *Appl. Phys. B* **128** 22
[23] Ronneberger O, Fische P and Brox T 2015 *International Conference on Medical Image Computing and Computer-assisted Intervention*, Cham, p. 234
[24] Zhang G, Guan T, Shen Z Y, Wang X N, Hu T, Wang D L, He Y H and Xie N 2018 *Opt. Express* **26** 19388
[25] Siddique N, Paheding S, Elkin C P and Devabhaktuni V 2021 *IEEE Access* **9** 82031
[26] Huang G, Liu Z, Van D M L and Weinberger K Q 2017 *IEEE Conference on Computer Vision and Pattern Recognition* (CVPR) July, 2017, p. 4700
[27] Hore A and Ziou D 2010 *International Conference on Pattern Recognition*, August 23–26, 2010, Istanbul, Turkey, p. 2366
[28] Xia P, Zhang L and Li F 2012 *Inf. Sci.* **307** 39
[29] Deng L 2012 *IEEE Signal Processing Mag.* **29** 141
[30] Xiao H, Rasul K and Vollgraf R 2017 arXiv: 1708.07747 [cs.LG]
[31] Kuzmenko A, Iezhov P and Kim J 2011 *Digital Holography and Three-Dimensional Imaging.* DTuC37
[32] Chen L Z, Zhang H, He Z, Wang X Y, Cao L C and Jin G F 2020 *Appl. Sci.* **10** 3652